# Analysis of zero-point electromagnetic energy and Casimir forces in conducting rectangular cavities

G. Jordan Maclay*

*Quantum Fields LLC, 20876 Wildflower Lane, Richland Center, Wisconsin 53581*

The goal in this effort is twofold: (1) to develop an understanding of Casimir forces in geometries more complicated than the usual parallel-plate geometry and (2) to provide extensive numerical computations to elucidate quantitative and qualitative aspects of the vacuum fluctuation energy and Casimir forces for the rectangular cavity. We review geometries for which Casimir forces and vacuum energy have been computed, and point out some of the difficulties with the ideal-conductor boundary conditions and ideal-shape boundary conditions, e.g., infinitely sharp edges. We investigate the vacuum electromagnetic stress-energy tensor at 0 K for a perfectly conducting three-dimensional rectangular cavity with sides $a_1 \times a_2 \times a_3$. The elements of the tensor are averaged over the appropriate spatial coordinates of the cavity. We first consider the average energy density $T^{00} = e(\boldsymbol{a})/V$ from the viewpoint of symmetry, where $e(a_1, a_2, a_3) = e(\boldsymbol{a})$ is the finite change in the zero-point energy from the free-field case. The vacuum energy $e(\boldsymbol{a})$ and the total vacuum force on the wall normal to the $i$ direction, $F_i = -\partial e/\partial a_i$, are both homogeneous functions of the cavity dimensions. Because of this symmetry, the energy and forces are related by the equation $e(\boldsymbol{a}) = \boldsymbol{a} \cdot \boldsymbol{F}(\boldsymbol{a})$. We compute the vacuum forces and energy numerically for cavities with a broad range of dimensions. The implications of the perfect-conductor boundary conditions and the effects of the edges of the cavity are both considered. The $C_{3v}$ symmetry of the constant-energy surfaces is apparent. The zero-energy surface, which is invariant under dilations and therefore extends to infinity, separates the nested, concave, positive-energy surfaces from the open, negative-energy surfaces. The positive- (negative-) energy surfaces are mapped into each other by scale changes. The force $\boldsymbol{F}(\boldsymbol{a})$ is normal to the constant-energy surface at $\boldsymbol{a}$. The surfaces corresponding to zero forces, $F_i(\boldsymbol{a}) = 0$, are invariant under dilations and are therefore infinite. The zero-energy surface and the zero-force surfaces delineate the different geometries for which there are zero, one, or two negative (inward or attractive) forces on the cavity walls, along with the sign of the corresponding energy. There is no rectangular cavity geometry for which all forces are negative or zero; conversely, only geometries that are not too different from a cube have all positive (outward or repulsive) forces. Only for the last case is the energy $e(\boldsymbol{a})$ necessarily positive. To provide an intuitive feeling for these vacuum energies, comparisons are made to other forms of energy in small cavities. We consider the energy balance for changes in cavity dimensions.

PACS number(s): 12.20.−m, 42.50.Lc, 03.70.+k

## I. INTRODUCTION

Casimir predicted the existence of an attractive force between two infinite parallel uncharged perfectly conducting plates in vacuum over 50 years ago [1]. This force arises because of the boundary conditions that the quantized source-free electromagnetic field must meet at the metal surfaces [2]. The prediction came very shortly after Bethe [3] and Welton [4] explained the Lamb shift in the hydrogen atom as due to interaction of the electron with the quantized vacuum electromagnetic field. The Casimir force was a startling and unexpected mesoscopic phenomenon arising from the presence of surfaces in the quantized vacuum field. The force was predicted to vary as the inverse fourth power of the separation between the plates. At a separation of 100 nm the predicted force/area was equivalent to about $10^{-4}$ atm; at 10 nm it was about 1 atm. The Casimir force has also been computed using the alternative language of source theory and radiative reaction, without explicit reference to vacuum fluctuations [5,6].

Since Sparnaay's first attempts in 1959, various measurements have been made on dielectrics [7] that have generally verified the theory of Casimir forces as developed for dielectrics [8], but not until quite recently was the existence of this attractive Casimir force between metallized surfaces verified, in two separate experiments. Lamoroux [9] used a torsion pendulum with an electromechanical feedback system to measure the Casimir force between a metallized spherical lens and a flat plate to an accuracy of about 5–10 % for separations of about 0.6–6 $\mu$m. Mohideen and Roy [10] used an atomic force microscope (AFM) to measure the force between a metallized optical flat and a metallized ball mounted on the AFM cantilever, obtaining a precision of about 1% for separations of 0.1–0.9 $\mu$m. As measured by the AFM, the forces on an effective area of approximately 10 $\mu$m$^2$ were in the piconewton range. Mohideen and Roy [10] included corrections for the surface roughness, the plasma frequency of the material, finite temperature, finite size and curvature of the surfaces, and instrumental effects.

With the advent of improved methods of making micron and submicron structures, such as microfabrication technology, it has become possible to explore forces arising from quantum fluctuations in greater detail. For example, the cantilever used by Mohideen and Roy [10] is a silicon micro-

---

*The web address of Quantum Fields LLC is www.quantumfields.com. Electronic address: jordanmaclay@quantumfields.com

TABLE I. Change in vacuum energy at 0 K for different perfectly conductive geometries (only cutoff-independent, geometry-dependent terms are included).

| Parallel plate (spacing $a$, infinite plates, energy in an area $L \times L$) | Cube (side $a$) | Sphere (radius $r$) | Cylinder (radius $r$, infinitely long, energy in length $L$) |
|---|---|---|---|
| $-0.0137 \hbar c L^2 / a^3$ | $+0.0916 \hbar c / a$ | $+0.0923 \hbar c / 2r$ | $-0.0156 \hbar c L / r^2$ |

machined device, often called a MEMS device (microelectromechanical system). The small separation between neighboring surfaces in various MEMS devices means it is possible that the presence of Casimir forces may result in adjacent surfaces being attracted to or sticking to each other [11]. Using micromachining methods, a variety of MEMS structures in which vacuum stresses are present can be fabricated. A harmonic oscillator with a Casimir interaction has been modeled but not yet built [12]. Some structures, including cavities, can be built to investigate Casimir forces especially using AFM methods [13].

Most of the discussions of the Casimir forces are given for the perfectly conducting, infinite-parallel-plate geometry, which is a very special and symmetric geometry. It contains no curved surfaces, such as right angles, and it retains Lorentz invariance in two of the three spatial directions [14]. It is common to explain the attractive Casimir force for this geometry: "Since the plates exclude vacuum radiation modes with wavelengths longer than twice the spacing, the energy density within the cavity is less than the energy density outside the plates. Hence the force is attractive." That this explanation is simplistic is clear when we consider that cubical or spherical cavities, which also exclude certain modes, have a positive energy density and positive (outward) forces (see Table I). In rectangular cavities, the energy density may be positive, negative, or zero depending on the ratio of the sides, while the forces may be outward, inward, or even zero. Forces depend on the derivative of the energy with respect to the corresponding direction, not on the sign of the energy density. If we examine the infinite-parallel-plate geometry more fully, and imagine placing perfectly conductive metal surfaces normal to the parallel plates in order to enclose the volume between the plates, then there would be outward forces on these additional four infinitely long, narrow surfaces [15].

Geometries with curved surfaces or intersecting planes present special problems with respect to vacuum energy [16,17], which we mention briefly since these issues have received little attention in the literature. Curved surfaces alter the local density of modes and the vacuum energy in the region near the surface. In general, the change in mode density from the free-field case that occurs very near a surface varies as the inverse of the radius of curvature [17]. This is a significant observation since it shows that conductive surfaces can yield a mode density greater than (as well as less than) that for the free field and it may provide some explanation for the appearance of positive as well as negative energy densities. For gently curved conductors, Deutsch and Candelas [16] have shown that the stress-energy tensor is approximately proportional to the sum of the reciprocals of

the two principal radii of curvature and varies inversely as the cube of the distance to the surface. It follows that the total vacuum energy in any compact region that contains part of the ideal curved conducting surface is infinite. For two perfectly conducting intersecting planes, Dowker and Kennedy [18] showed that the renormalized stress-energy tensor depends on the intersection angle and varies as the inverse fourth power of the distance from the intersection line. Again, it follows that any compact region containing part of the line of intersection contains an infinite (negative) vacuum energy contribution.

Lukosz [19] has computed the change in the vacuum energy due to the infinitely sharp edges of a perfectly conducting rectangular cavity. He finds a quadratically divergent term proportional to the perimeter of the cavity. For the physically relevant case of a finite radius of curvature $R \ll a_1, a_2, a_3$, the divergence vanishes and he obtains a correction to the total energy equal to $\delta E = A \hbar c (a_1 + a_2 + a_3) / R^2$, where $A$ is a constant of proportionality, which he does not compute, but notes it may be zero. The effect of this additional term $\delta E$, which depends on the radius of curvature, will be discussed.

The infinities that appear for ideal conductors represent a breakdown of the perfect-conductor approximation. The ether cannot store an infinite amount of energy (whether positive or negative) in a compact region, nor can the conductor support the infinite stresses. The perfect-conductor boundary conditions are pathological, and lead to an infinite physically observable gravitational field [14,16]. For a real metal the edges are not infinitely sharp, and the electrons are unable to follow an applied electromagnetic field at frequencies above the plasma frequency of the metal. Thus, for frequencies above the plasma frequency, the zero-point electromagnetic field is not effectively altered by the presence of the conductive plates and the boundary conditions for an ideal conductor are not met.

When a wavelength cutoff corresponding to finite plasma frequency is included, then the infinities in the stress-energy tensor disappear. However, the question then arises whether the use of a cutoff produces terms in the vacuum energy that depend on the molecular properties through the plasma frequency, and further, whether these terms depend on the geometry or not. To date, only the sphere has been analyzed in detail, with the result that a geometry-independent, cutoff-dependent term has been found [20]. Since this term is geometry independent, it will not affect the computation of the vacuum stress from the vacuum energy.

Lifshitz [8] has developed a general theory of Casimir forces in terms of a frequency-dependent complex permittiv-

ity that can be applied to imperfect conductors or dielectrics. For metals such as aluminum, copper, or silver, the first-order theory predicts a reduction in the ideal perfect-conductor Casimir force of approximately 10% if the spacing is greater than the wavelength corresponding to the plasma frequency [21].

The total Casimir force on a surface cannot be accurately obtained by adding differential contributions from different regions of the surface. Instead, the geometry as a whole must be considered because it determines the modes of the vacuum electromagnetic field fluctuations that are present within the geometry [22]. The different modes determine the energy within the cavity and the derivative of the energy determines the force.

Vacuum energy and Casimir forces have been computed for several simple symmetric geometries aside from the parallel-plate geometry, as shown in Table I. For a conducting spherical shell [23,24] and a conducting hollow cube [25] the predicted Casimir forces are repulsive or outward. The vacuum stress on two intersecting planes is attractive. For conductive rectangular cavities with square cross section $1\times1\times c$), the Casimir energy and the forces on the cavity walls have been computed [25–27], with the result that the forces can be inward or outward depending on the specific dimensions. For example, the energy is positive in the interval [28]

$$0.408 < c/a < 3.48$$

and zero at the endpoint of this interval, and negative outside the interval. Ambjorn and Wolfram [26] have computed the constant-energy contours for $a_1\times a_2\times a_3$ geometry for the region $a_2, a_3 > 1$.

The four different computations of the stress-energy tensor (referenced in the previous paragraph) for special cases of a conductive rectangular cavity were done using a variety of methods as discussed in Sec. II. These calculations all agree with each other, although none of the calculations has explicitly included the vacuum energy associated with the right angles. Hacyan *et al.* [27] identified two divergent terms, one proportional to the perimeter of the cavity and a second term proportional to the volume. The term Lukosz [19] identified as a divergent correction to the energy for the case of a perfect rectangular cavity with infinitely sharp corners appears to correspond to the divergence of Hacyan *et al.* [27] that is proportional to the perimeter. For the real corners, the correction to the energy for the effect of a finite radius of curvature is finite and equal to the finite correction $\delta E$.

To get some idea of the scale of the Casimir energy in terms of familiar quantities, we can rewrite the equation for the vacuum energy in a cube (Table I) in terms of the Compton wavelength $\lambda_C$ and mass $m$ of the electron,

$$E_C = 0.0916(\lambda_C/a)mc^2, \tag{1}$$

or in terms of the energy $E_{\text{ph}}$ of the longest-wavelength photon ($\lambda = 2a$) that just fits in the cavity,

$$E_C = (0.0916/\pi)E_{\text{ph}}. \tag{2}$$

For cubes with sides of 100 and 0.1 nm, respectively, the vacuum energies are 0.18 and 180 eV. The corresponding pressures are $0.9\times10^{-4}$ and $0.9\times10^8$ atm. These pressures are equivalent to the blackbody radiation pressure ($bT^4/3$) at temperatures of $1.3\times10^4$ and $1.3\times10^7$ K, respectively. Although the vacuum energy density in this example is small by some scales, it increases rapidly as dimensions decrease and is about $4\times10^8$ and $4\times10^{20}$, respectively, times as large as the energy density of an infinite photon gas at room temperature.

There is no easy way to understand the geometrical dependence of the vacuum stress and energy. Schwinger *et al.* have described the Casimir force between uncharged conductors as ''one of the least intuitive consequences of quantum electrodynamics [29].'' In a recent review article describing ways of computing vacuum energy and the Casimir effect, a section was titled ''The mystery of the Casimir effect'' [30]. In an effort to gain some understanding of the Casimir effect, particularly the geometrical dependence of the force, we have explored the conductive rectangular cavity in some detail, paying attention to the fundamental concepts and the symmetries, and to analyzing and graphing the three-dimensional computations. We have performed numerical computations of the vacuum energies and Casimir forces for the general case of a cavity with sides $a_1, a_2$, and $a_3$.

The organization of the paper is as follows. In Sec. II we present the details of the numerical calculations of the vacuum energy $e(\boldsymbol{a})$ and forces $\boldsymbol{F}(\boldsymbol{a})$. In Sec. III we consider the nature of the vacuum energy and stresses in a rectangular cavity with sides $a_1, a_2, a_3$, including the implications of the geometrical symmetry. In this section, we illustrate the general results using figures based on the calculations of Sec. II, which show constant-energy surfaces, constant-force surfaces, and contours. In Sec. IV we give a brief conclusion.

## II. COMPUTATION OF THE VACUUM ENERGY AND VACUUM FORCES

The vacuum energy $e$ at 0 K, given as a function of the dimensions of a rectangular box with perfectly conductive sides of length $\boldsymbol{a}\equiv(a_1,a_2,a_3)$, is $e(a_1,a_2,a_3)\equiv e(\boldsymbol{a})$. This energy represents the change in the zero-point vacuum energy due to the presence of the conductive surfaces of the box. We do not consider the variation of the energy density with position within the cavity. Formally, the vacuum energy $e(\boldsymbol{a})$ is computed as the total vacuum energy with the box present minus the total vacuum energy when the box dimensions go to infinity. By defining the energy in this manner, the free-field vacuum energy divergence can be made to cancel by suitable mathematical procedures and a finite result for $e(\boldsymbol{a})$ is obtained.

Ambjorn and Wolfram [26] derived an expression for the change in the vacuum energy $e(\boldsymbol{a})$ due to a perfectly conductive rectangular box with sides $(a_1,a_2,a_3)$ by summing the eigenmodes. The divergent sums were regularized by using analytic continuation in the dimensionality of the cavity and the result was given in terms of the Epstein Zeta function [31]. From their equations, and the definition of the standard

Zeta function, one can show that for the case of electromagnetic radiation in a three-dimensional cavity, the Casimir energy is given by

$$e(a_1,a_2,a_3) = -(\hbar c/16\pi^2)[a_1 a_2 a_3 \zeta(a_1,a_2,a_3;4)$$
$$-(\pi^3/3)(1/a_1 + 1/a_2 + 1/a_3)], \quad (3)$$

where this form of the Epstein Zeta function is defined by

$$\zeta(a_1,a_2,a_3;s) = \sum_{n_3}^{\infty} \sum_{n_2}^{\infty} \sum_{n_1}^{\infty} [(a_1 n_1)^2 + (a_2 n_2)^2$$
$$+ (a_3 n_3)^2]^{-s/2}. \quad (4)$$

The sum is over all values of $n_1,n_2,n_3$ except when all indices equal zero. This Zeta function is absolutely convergent for nonzero $a_i$ if $s>3$, in which case the terms may be summed in any order as long as all terms are included [32]. The energy $e(a)$ is finite as long as each side $a_1,a_2,a_3$ is nonzero. There is a manifestly negative contribution to $e(a)$ given by the Zeta function, and a manifestly positive contribution given by the second term, which is proportional to the area/volume of the cavity. To give a sense of scale, we note that this positive term equals $\frac{1}{48}$ times the total energy of the three longest-wavelength photons that can fit in the cavity ($\lambda_i = 2a_i$). Mathematically, the positive term occurs because modes in which two of the three indices $n_1,n_2,n_3$ are zero cannot propagate within the cavity (the fields vanish), and therefore cannot contribute to the energy. This term equals $-\frac{1}{2}$ of the sum of the zero-point energies of one-dimensional resonators of length $a_1,a_2,a_3$, respectively [25]. If one (or two) of the dimensions is much larger than the other dimension(s), then the second term becomes negligible, and the energy is always negative and depends on only the smaller sides [33]. The Zeta function term has been interpreted as arising from the multiple reflections of virtual photons traveling perpendicular to the walls in periodic orbits [33].

This expression for the energy, Eq. (3), agrees exactly with that obtained by Lukosz [25], who summed all the modes in the cavity and employed an exponential convergence factor. The justification for the validity of the convergence factor was provided by the generalized Weyl theorem, which states that the eigenfrequency density per unit volume of the resonator is independent of the size and form of the resonator for frequencies much higher than the fundamental eigenfrequency. A third calculation for cavities is provided by Hacyan *et al.* [27], who obtained expressions for the stress-energy tensor from the Fourier transforms of the correlation functions for the quantized electromagnetic field. This process allowed them to isolate and remove the divergences. They did numerical calculations of components of the stress-energy tensor in configuration space for a $1 \times 1 \times c$ cavity which are in agreement with Eq. (3) and our results. This agreement shows that our application of the principle of virtual work to calculate forces from the energy is justifiable. Mostepanenko and Trunov [28] also report results for the special case of $a_1 = a_2$ that are in agreement with our formulation above.

In this paper, we evaluate Eq. (3) for $e(a)$ to compute the energies for arbitrary dimensions $(a_1,a_2,a_3)$. The evaluation was done using an algorithm developed by Crandall and Buhler [34]. To secure accurate sums, this algorithm uses direct summation in which progressively larger sets of terms are averaged together as $n_i$ increases. In principle, the accuracy of each calculation should be to order $[\exp(-9\pi)] \approx 5 \times 10^{-13}$. In all computations we set $\hbar = c = 1$. The figures do not include the effect of the correction term $\delta E$, which depends on the radius of curvature, since we do not know the constant of proportionality.

Most of the graphs are based on computations of $e(a_1,a_2,a_3)$ for values of $a_1$, $a_2$, and $a_3$ between 0.1 and 4.0, with a mesh of 0.1. Derivatives were computed numerically to first order. Equation (14) was used to check the consistency of the computations. The first few points near the beginning of the interval (values of $a_1,a_2,a_3$ in the range 0.1 to 0.3) show a small error; the remaining points do not show significant error. The computations were done on a Dell XPS R450 450 MHz computer with 384 megabytes of RAM, and took several weeks running 24 h/day to finish.

## III. NATURE OF THE VACUUM ENERGY AND STRESS

The energy difference $e(a)$ can depend only on the lengths of the sides (assumed to be positive), on Planck's constant $\hbar$, and on the speed of light $c$. From dimensional consideration, the energy $e$ must be proportional to $\hbar c$ times $f(a)$, where the function $f(a)$ has the dimensions of inverse length:

$$e(a) = \hbar c f(a). \quad (5)$$

Since the energy cannot depend on the choice of axes, the dependence of $e(a)$ on $a_1$ must be identical to the dependence on $a_2$ or $a_3$. Hence the function $f(a_1,a_2,a_3)$, as well as the function $e(a_1,a_2,a_3)$, which is proportional to $f(a_1,a_2,a_3)$, are homogeneous functions of $a_1$, $a_2$, and $a_3$ of degree $-1$:

$$e(\lambda a_1, \lambda a_2, \lambda a_3) = \lambda^{-1} e(a_1,a_2,a_3). \quad (6)$$

This property allows us to calculate values of the energy for arguments that are proportional. It also indicates that the surfaces of constant energy will be nested as a function of the energy, with higher energies for smaller cavities. All surfaces of constant positive energy are identical with a uniform dilation $a \to \lambda a$; similarly all surfaces of constant negative energy are identical with a scale change. For example, if the energy corresponding to a constant-positive-energy surface is doubled, then the dimensions for the new surface are cut in half. The zero-energy surface is unique in that scale changes map it into itself, which means the surface must extend to infinity, separating the negative- and positive-constant-energy surfaces.

The energy $e(a)$ will be unchanged if any two dimensions, for example, $a_1$ and $a_2$, are interchanged by a reflection. In addition, a rotation by $+120°$ about the symmetry axis $a_1 = a_2 = a_3$ results in the cyclic permutation $a_1 \to a_2$, $a_2 \to a_3$, $a_3 \to a_1$, which leaves the energy unchanged. (Ro-

tations or reflections in which the values of $a_1$, $a_2$, or $a_3$ can assume negative values are not allowed. The point $a=0$ must remain unchanged.) The symmetry group corresponding to these geometrical transformations is $C_{3v}$, where the $C$ indicates "cyclic," the 3 indicates a threefold axis of symmetry, and the $v$ indicates the presence of three vertical planes of symmetry through the symmetry axis. The molecules $NH_3$ and $ClCH_3$ are members of this symmetry group. Each surface of constant energy displays the $C_{3v}$ symmetry and is a one-dimensional representation of this group [35]. The transformation of the constant-energy surfaces under dilations constitutes an additional symmetry.

### A. Constant-energy surfaces

It is useful to consider the special case of a cube in order to derive some general results about constant-energy surfaces for positive and negative energies. For the special case of a cube, the energy dependence collapses from $e(a_1,a_2,a_3)$ to $e(a,a,a)$ and for dimensional reasons discussed above $e$ must be proportional to $1/a$. The constant of proportionality in $e$, which must be obtained by direct computation, is shown in Table I.

For every positive energy $E_p$, there is a corresponding cube that has that energy. The axis of symmetry ($a_1=a_2=a_3$) must intersect the constant-energy surface for $E_p$ at the point that corresponds to this cube. At this point, the surface is normal to the axis of symmetry since $F_1=F_2=F_3$. From the homogeneity and symmetry of $e(a)$, it follows that all the surfaces of constant positive energy are continuous, nested or nonintersecting surfaces that close on themselves for positive $a$. The zero-energy surface separates all positive-energy surfaces from the negative-energy surfaces. This also implies that all negative-energy surfaces will be open, nested surfaces. It also follows that for all rectangular cavities with a given positive energy, the cube is the one with the longest main diagonal. The statements in this paragraph are valid whether we are talking about energy density or energy.

In order to illustrate these results, we present some of the figures based on the computations described in Sec. II. Figure 1 shows two views of the surface $S_0$ corresponding to zero vacuum energy for values of the sides up to 4. (We use natural units in which $\hbar=c=1$.) Figure 2 shows a separate computation of the zero-energy surface for values up to 10. The surfaces in both these figures show the rotational and reflection symmetry of the group $C_{3v}$ discussed above. In addition, the zero-energy surface is seen to be invariant under dilation. Figure 3 shows a positive-energy surface from two different views to display unambiguously the symmetry of the surface. Figures 4–6 show different sets of nested negative- and positive-energy surfaces, from different observation points. Portions of the surfaces for values of $a_1,a_2,a_3>4$ are not plotted, resulting in the holes in the $e$ $=0.025$ surface in Fig. 6. All positive- (or negative-) energy surfaces are similar and can be obtained from each other using the dilation operation because $e(a)$ is a homogeneous function. All constant-energy surfaces approach the origin as $a\rightarrow 0$ but do not converge to it. When the origin is viewed
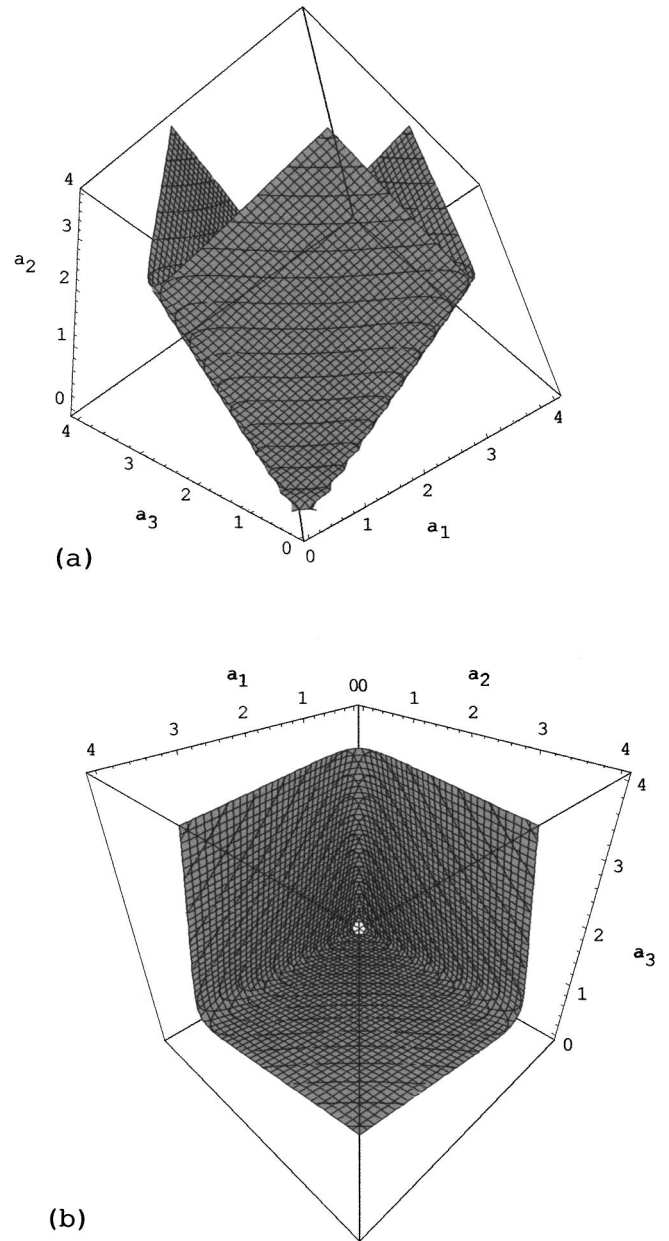


(a)



(b)

FIG. 1. Surface of zero energy $e(a)=0$ plotted for values $a_1,a_2,a_3<4$. In (a) the surface is plotted with the symmetry axis $a_1=a_2=a_3$ vertical; in (b) the surface is plotted with the viewpoint along the symmetry axis.

from along the axis of symmetry, a small hexagonal opening in the constant-energy surface surrounds the origin [Fig. 1(b)].

One of the advantages of working in terms of constant-energy surfaces is that they provide a geometrical interpretation of the vacuum forces. From the first-order theory of functions, the change $de$ in the vacuum energy in the cavity that occurs when we move a distance $da$ is given by

$$de=da\cdot\nabla_a e(a), \qquad (7)$$

where the gradient is taken with respect to $(a_1,a_2,a_3)$. Physically, this equation represents the principle of virtual
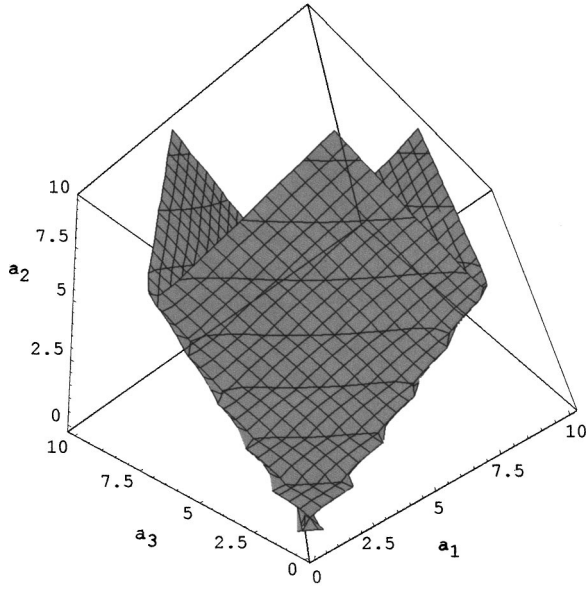
FIG. 2. Surface of zero energy $e(\boldsymbol{a}) = 0$ plotted for values $a_1, a_2, a_3 < 10$. The roughness along the sides of the surface is an artifact due to the coarseness of the mesh. The surface is the same shape as that in Fig. 1.

work, in which the differential change in vacuum energy in the cavity equals the sum of the external forces exerted on the cavity walls times the differential changes in the corresponding dimension. The external force on each wall equals the negative of the force on the walls of the cavity due to vacuum fluctuations. Thus we identify

$$\boldsymbol{F}(\boldsymbol{a}) = -\boldsymbol{\nabla}_a e(\boldsymbol{a}), \tag{8}$$

where the component $F_1 = -\partial e / \partial a_1$ is the total vacuum force on the face normal to the $a_1$ direction, etc. The average pressure in the $a_1$ direction is $F_1/(a_2 \times a_3)$. The energy $e(\boldsymbol{a})$ decreases most rapidly in the direction of the force $\boldsymbol{F}(\boldsymbol{a})$. The conservation of energy that occurs when the dimensions of the cavity are altered quasistatically is represented by

$$de = -d\boldsymbol{a} \cdot \boldsymbol{F}(\boldsymbol{a}). \tag{9}$$

Consider a surface $S_K$ of constant energy $K$ defined by

$$K = e(\boldsymbol{a}). \tag{10}$$

If the displacement $d\boldsymbol{a}$ is tangent to the surface of constant energy, then the corresponding change in energy vanishes and

$$0 = d\boldsymbol{a} \cdot \boldsymbol{F}, \tag{11}$$

which implies the important result that the vacuum force $\boldsymbol{F}(a_1, a_2, a_3)$ corresponding to the cavity with sides $(a_1, a_2, a_3)$ must be perpendicular to the surface $S_K$ of constant energy at $(a_1, a_2, a_3)$ [36]. The relationship is also obeyed by the correction $\delta E = A\hbar c (a_1 + a_2 + a_3)/R^2$ to the energy for a finite radius of curvature $R$. The surface of constant $\delta E$ is a plane perpendicular to the main diagonal of the cavity. From Eq. (8) we find that $\delta E$ yields a constant force
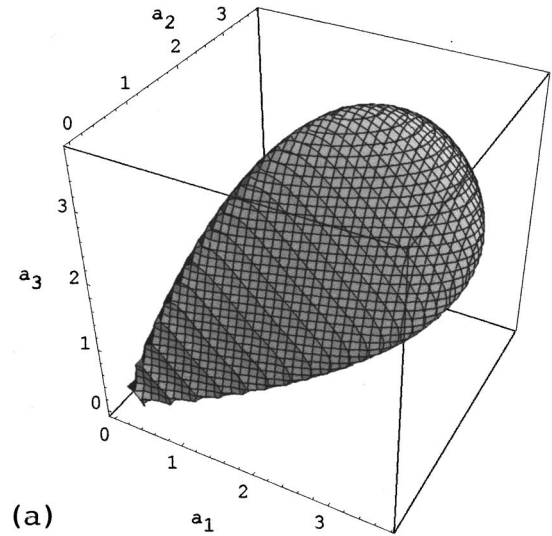


**(a)**
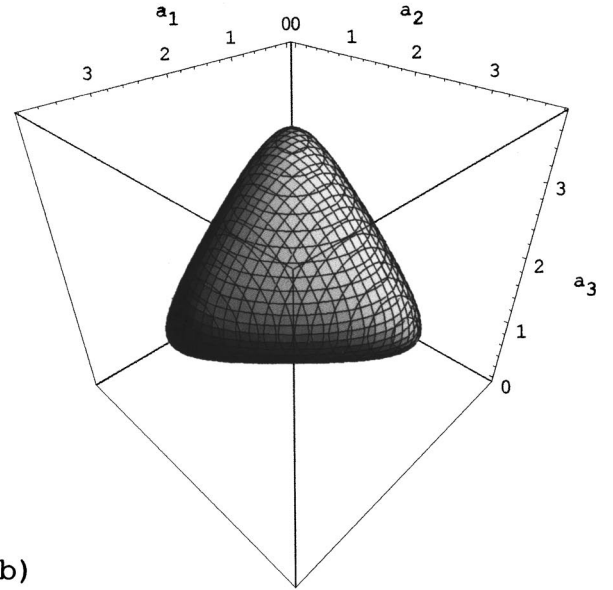


**(b)**

FIG. 3. Constant-energy surface with $e(\boldsymbol{a})$ equal to 0.03. In (a) the surface is viewed from the side; in (b) the surface is viewed from along the symmetry axis.

$\delta F = A\hbar c/R^2$ direct along the main diagonal of the cube, perpendicular to the constant-energy surface.

The components of the averaged stress-energy tensor as functions of $\boldsymbol{a}$ are given as [37]

$$\langle T^{00}(\boldsymbol{a}) \rangle = e(\boldsymbol{a})/V,$$

$$\langle T^{11}(\boldsymbol{a}) \rangle = F_1(\boldsymbol{a})/a_2 a_3 = -(1/a_2 a_3)\partial e(\boldsymbol{a})/\partial a_1$$
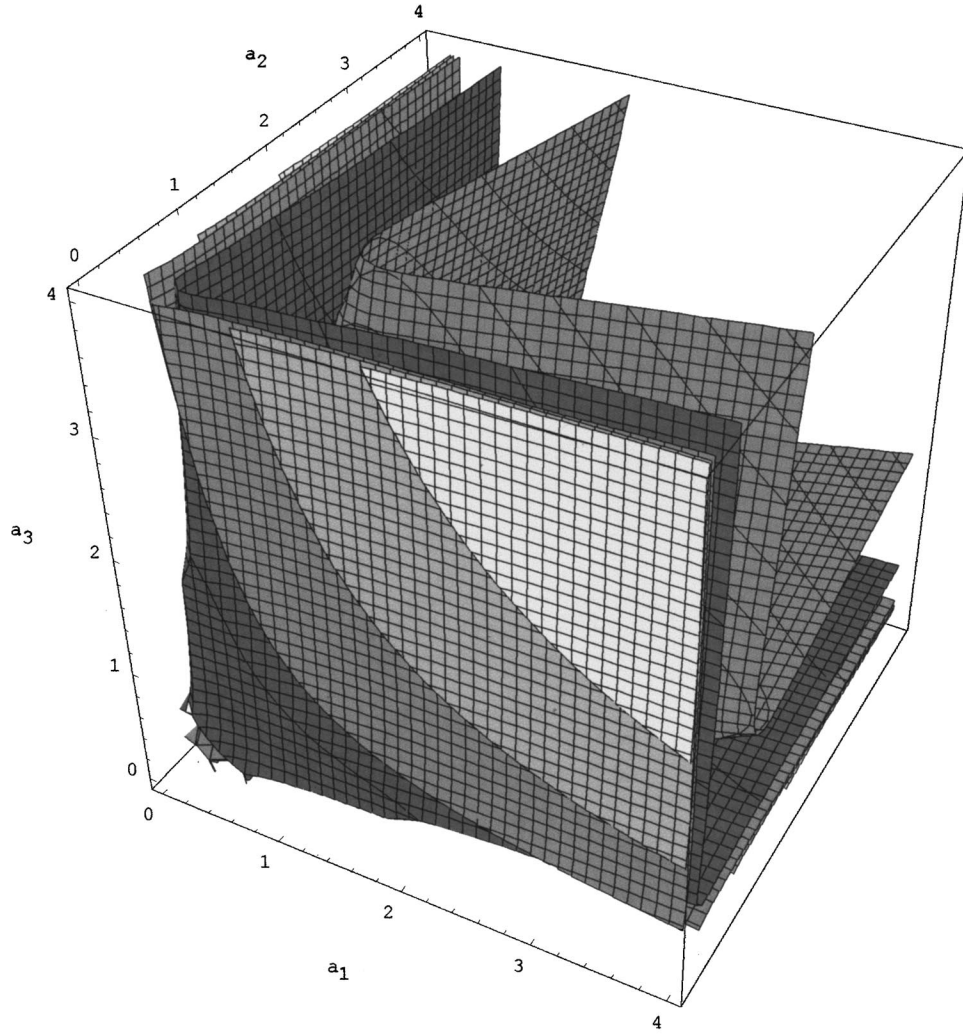
(and cyclic permutations). (12)

FIG. 4. Set of nested surfaces of constant energy plotted for $a_1, a_2, a_3 < 4$. The values of $e(\boldsymbol{a})$ are $-100, -50, -20, -1, 0.0$. The energy increases as the surfaces get closer to the symmetry axis.

The averaged stress-energy tensor has no dependence on $x, y, z$ since we have averaged over the volume $V$ of the cavity, or averaged over the area of a face. The off-diagonal terms, which contain sine and cosine functions, vanish after averaging. The divergence of the stress tensor vanishes within the cavity, as it must, since the electromagnetic field is free except at the boundaries. Since the photon is massless, there is no intrinsic unit of length, and the theory is invariant under scale transformations of the electromagnetic field strength. This invariance is reflected in the vanishing of the trace of the stress-energy tensor [15].

We can demonstrate directly that the stress-energy tensor defined in Eq. (12) has zero trace by applying Euler's theorem for homogeneous functions [38]. This theorem states that for a homogeneous function $f(\boldsymbol{x})$ of degree $p$, $f(\lambda \boldsymbol{x}) = \lambda^p f(\boldsymbol{x})$, and we have

$$\boldsymbol{x} \cdot \boldsymbol{\nabla}_x f(\boldsymbol{x}) = p f(\boldsymbol{x}). \qquad (13)$$

Applying Euler's theorem to $e(\boldsymbol{a})$ we obtain

$$\boldsymbol{a} \cdot \boldsymbol{F}(\boldsymbol{a}) = e(\boldsymbol{a}). \qquad (14)$$

If we write this equation in components and divide by the volume, we find that the trace of the stress-energy tensor vanishes identically.

Equation (14) also shows that the energy in the cavity can be interpreted as the sum of the products $a_i F_i$ of the force on each side times the length of that side. This result, which is a form of the mean-value theorem applied to the conservation of energy, helps explain some of the results obtained for rectangular cavities, for example, the following. (1) Cavities with zero total energy must have positive forces on one or more faces and negative forces on one or more faces. (2) Cavities with negative (positive) total energy must have a negative (positive) force on at least one side. (3) Cavities with all positive forces must have positive energy. If we apply Eq. (14) to a cube, we obtain a force $F(a) = e(a)/3a$ on each face. This result is comparable to the usual result for the isotropic pressure $p$ of an infinite photon gas in terms of
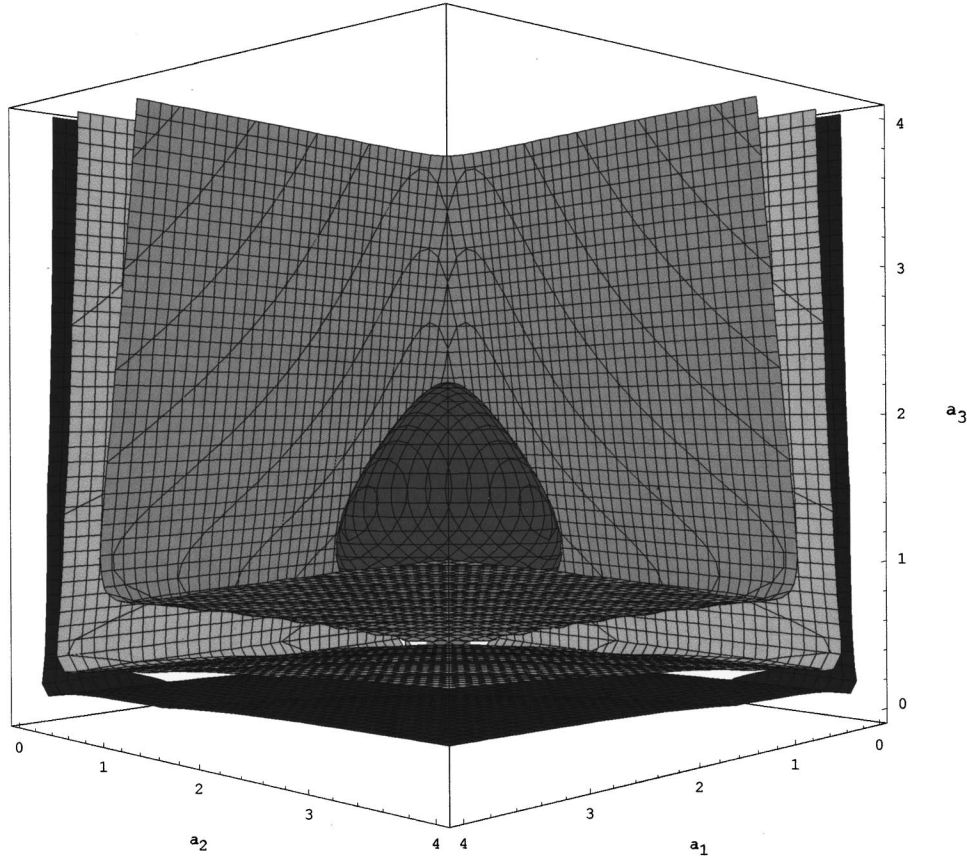
FIG. 5. Set of nested surfaces of constant energy $e(\boldsymbol{a})$ equal to $-10, -1, -0.05, 0.05$, plotted for $a_1, a_2, a_3 < 4$. The most negative surfaces are closest to the axes.

its energy density $U$, namely, $p = U/3$. In the general case the energy within the cavity is not isotropic.

### B. Constant-energy contours and energy surfaces

Two-dimensional contour plots of constant energy can be obtained by taking cross sections of the constant-energy surfaces such as are shown in Figs. 4–6. If we take cross sections with constant values of $a_3$, we obtain the constant-energy contours, given as functions of $a_2$ and $a_3$, in Fig. 7, for $a_3 = 0.5, 1.0, 3.5$. The dark line in each graph shows the zero-energy contour. The maximum energy in the contours occurs for the geometries $0.3 \times 0.3 \times 0.5$, $0.6 \times 0.6 \times 1.0$, and $2.1 \times 2.1 \times 3.5$, respectively. The contours do not show the rotational symmetry of the constant-energy surfaces because the planes with constant $a_3$ cut through the constant-energy surfaces at an angle. Ambjorn and Wolfram [26] reported that, for a contour with $a_3 = 1.0$, the maximum energy would occur for $1 \times 1 \times 1$. However, based on their graph, they did not consider values of $a_1$ and $a_2$ less than 1. Hacyan *et al.* [27] reported a maximum energy for a $1 \times 1 \times a_3$ box when $a_3 = 0.57$ that is in agreement with our calculations ($1/\sqrt{3}$).

It is useful to consider the constant-energy surfaces in a coordinate system that explicitly displays their $C_{3V}$ symmetry. One such coordinate system can be obtained by a Euler rotation, rotating by $-45°$ about the $a_3$ axis and then by $\cos^{-1}(1/\sqrt{3})$ about the new $a_1'$ axis. The equations of trans-

formation to the $(a_1', a_2', a_3')$ system are

$$a_1' = (1/\sqrt{2})(a_1 - a_2),$$

$$a_2' = (1/\sqrt{6})(a_1 + a_2) - \sqrt{(2/3)} a_3, \tag{15}$$

$$a_3' = (1/\sqrt{3})(a_1 + a_2 + a_3).$$

This rotation takes the symmetry axis $a_1 = a_2 = a_3$ into the $a_3'$ axis in the rotated system. Thus the $a_3'$ axis is the axis of symmetry of the constant-energy surfaces. To obtain the energy contours in the primed system for a constant value of $a_3'$, we plot the locus of points for which $e(a_1', a_2', a_3')$ has constant values and where $a_1 + a_2 + a_3 = \text{const} = (\sqrt{3}) a_3'$. This locus of points will lie in a plane in both coordinate systems. All the points on this plane of constant $a_3'$ correspond to boxes that have the same unvarying perimeter. Figure 8 shows two-dimensional contour plots of the energy in the primed system for $a_3' = 0.8$, 1.75, and 3. In Fig. 8(a), the region near the point $(0', 0')$ corresponds to the maximum energy $e = 0.19$, which is the energy of a cube of side $a_3'/\sqrt{3} = 0.46$. Similarly in Fig. 8(b), $a_3' = 1.75$ and the maximum energy corresponds to the contour $e = 0.09$ near the center.

The energy contours in the rotated system lie in the plane perpendicular to the axis of symmetry and therefore show
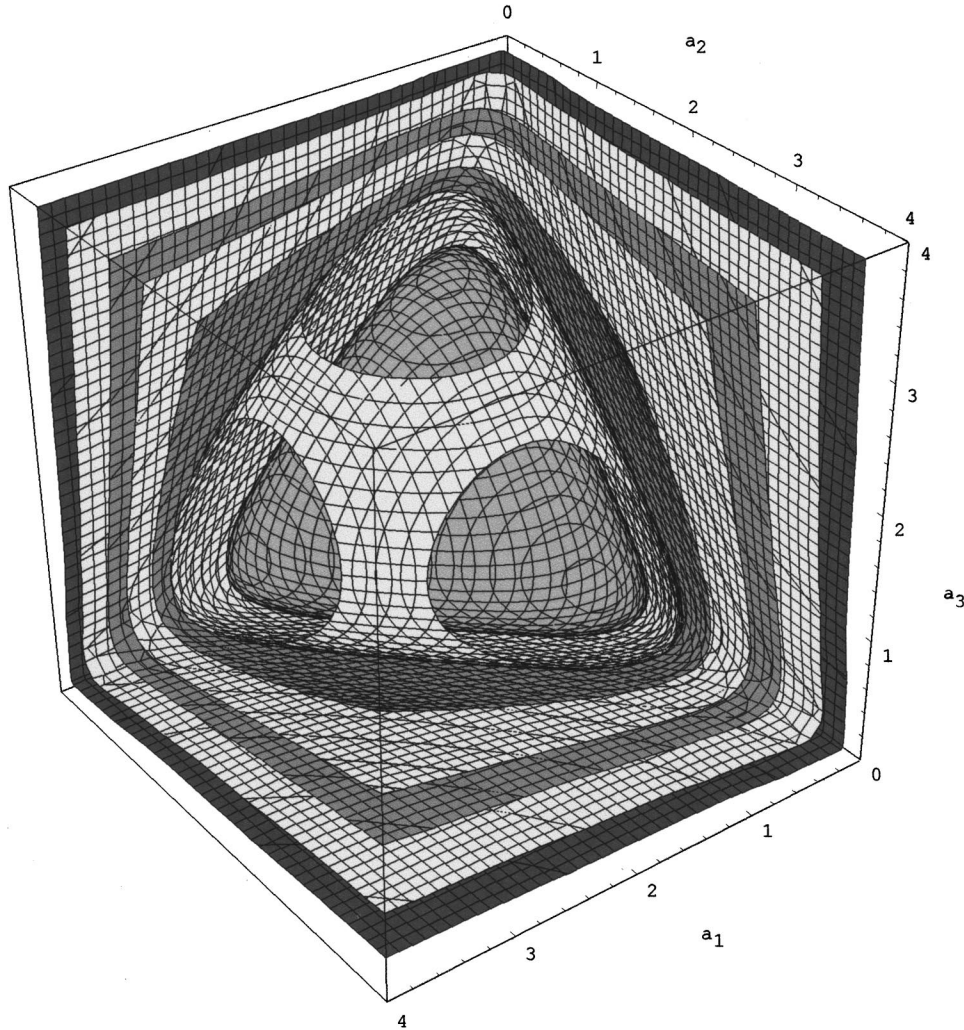
FIG. 6. Set of nested surfaces of constant energy $e(\mathbf{a})$ equal to $-5, -0.5, -0.05, 0.0, 0.02, 0.025, 0.03$, with the most negative surfaces closest to the axes.

$C_{3V}$ symmetry about the origin. The maximum positive energy for each plane will be the point $(0', 0')$ that corresponds to the cube $(0', 0', a_3')$, which is a cube with side $a = a'/\sqrt{3}$. The symmetry plane determined by $a_3' = \text{const}$ is tangent to the constant-energy surface corresponding to this cube at the point $(0', 0', a_3')$. The constant-energy surfaces for higher-energy cubes are smaller and so will not intersect the plane normal to the symmetry axis. The surfaces for smaller energies will be larger and therefore intersect the symmetry plane. Thus, for boxes with a constant perimeter, the cube has the largest positive energy. The largest negative energy is unbounded, since we may make one side arbitrarily small, and $e(\mathbf{a})$ becomes arbitrarily large and negative. In this primed coordinate system, the correction $\delta E$ to the energy for a finite radius of curvature can be written as $\delta E = A\hbar c(a_3')/R^2$.

As an alternative to two-dimensional energy contour plots, we can employ a three-dimensional plot in which the energy $e(\mathbf{a})$ is given as a function of $a_1$ and $a_2$ for fixed values of $a_3$. Figure 9 shows the plots of the energy $e(a_1, a_2)$ for $a_3 = 0.5, 1.0, 3.5$. These figures correspond to

the contour plots of Fig. 7. The sharp changes in energy for small values of $a_1$ and $a_2$ correspond to the "pizza box" geometries.

### C. Approximate form of zero-energy surface

The zero-energy surface $S_0$ (Fig. 1) separates the positive- and negative-energy surfaces. Much of the behavior of the cavity is governed by this surface. Its shape can be approximated as three planes, with their corners held at the origin, and tilted by an angle toward the line $a_1 = a_2 = a_3$. The question arises, what governs the tilt of these planes? Consider the vector $\mathbf{a}$, which goes from the origin to any point on $S_0$. The angle $\Phi_3$ that the vector $\mathbf{a}$ makes with the $a_3 = 0$ plane is

$$\Phi_3 = \tan^{-1}\{a_3/[(a_1)^2 + (a_2)^2]^{1/2}\}. \tag{16}$$

From symmetry, we take $a_1 = a_2 = a$ and obtain the angle of the tilted plane
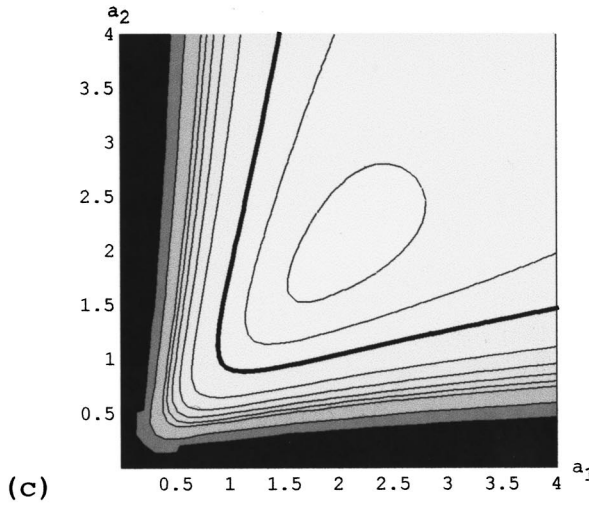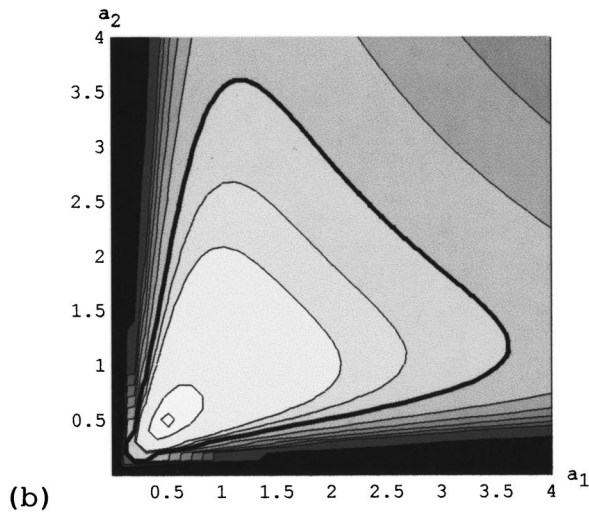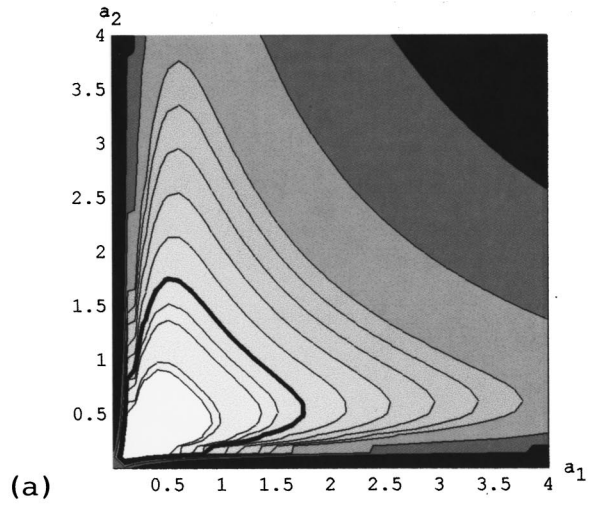
$$\Phi_3 = \tan^{-1}[a_3/a\sqrt{2}]. \tag{17}$$

(a)



(b)



(c)



(a)



(b)



(c)

FIG. 7. Contours of constant energy $e(\boldsymbol{a})$ as a function of $a_1$ and $a_2$ for $a_3$ = (a) 0.5, (b) 1.0, (c) 3.5. The contours correspond to values of $e = 0.111, 0.1, 0.05, 0.03, 0.0, -0.05, -0.1, -0.15, -0.2, -0.25, -0.5, -1.0$. (Not all contours are present for every plot.) The zero-energy contour is the heavy black line. Positive-energy contours lie within the zero-energy contour.
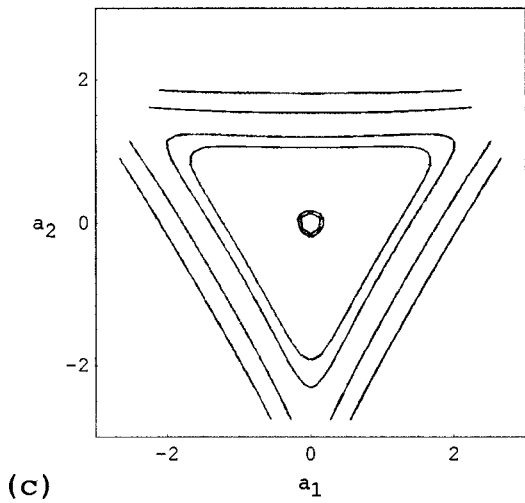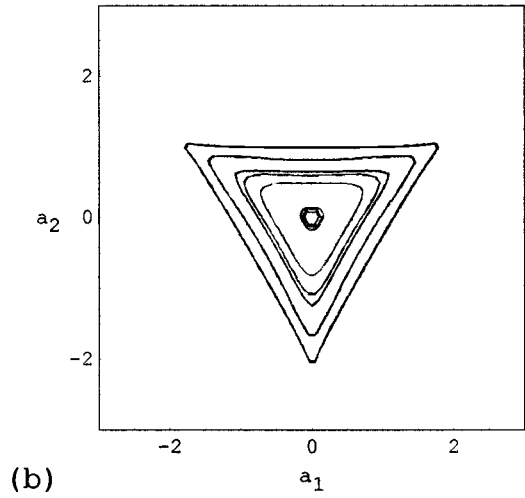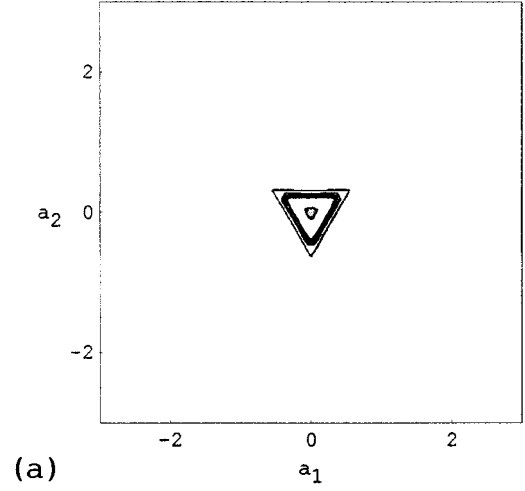
FIG. 8. Contours of constant energy $e(\boldsymbol{a})$ for $a_3' =$ (a) 0.8, (b) 1.75, (c) 3.0. These contours are in a rotated coordinate system in which the new $a_3'$ axis is the axis of symmetry. The contours correspond to values of $e(\boldsymbol{a})$ equal to $-5.0, -0.5, -0.05, 0, 0.052, 0.9, 0.2$. Not all contours appear in each plot.

## D. Constant-force surfaces

The components $F_i(\boldsymbol{a})$ of the total vacuum force are first-order partial derivatives of $e(\boldsymbol{a})$, which is a homogeneous function of degree $-1$, and the $f_i(\boldsymbol{a})$ are therefore homogeneous functions of degree $-2$:

$$F_i(\lambda a_1, \lambda a_2, \lambda a_3) = \lambda^{-2} F_i(a_1, a_2, a_3). \qquad (18)$$

The surface that corresponds to the constant force $F_i = 0$ will transform into itself under scale changes for arbitrarily large $\lambda$, and must therefore extend to infinity, separating the region in which $F_i$ is positive from the region in which $F_i$ is negative. The region of space that includes the line $a_1 = a_2 = a_3$, corresponding to a cubic geometry, is the domain of all positive forces $F_i$.

In Fig. 10(a), we show the surface corresponding to the constant force $F_3 = 0$. In the regions closest to the plane $a_3 = 0$, the force $F_3$ is negative; on the other side of the surface the force is positive. In Fig. 10(b), the three surfaces $F_1 = 0$, $F_2 = 0$, $F_3 = 0$ are plotted. These surfaces define the various cavity geometries for which the forces are positive or negative or zero. The intersection of two of these surfaces defines a set of geometries $(a_1, a_2, a_3)$ for which, for example, $F_1 = F_2 = 0$. In this region, $F_3 > 0$, so the energy must be positive. The central conical region corresponds to approximately cubical boxes for which all three forces are positive, and for which [by Eq. (14)] the energy is also positive. The largest regions, near each plane $a_i = 0$, have two forces positive and one negative, and correspond to geometries ranging from a cake box to a pizza box (the one side which is smaller than the other two sides experiences the negative or attractive force). In the limit of a thin, large, square pizza box, the energy density is negative, the attractive pressure is three times the energy density, and the repulsive pressures are both minus the energy density [15]. In the three narrow regions bounded by the intersection of two surfaces, two forces are negative, one positive. These regions correspond to toothpaste boxes that have an approximately square cross section, with a longer third side. The longer sides experience approximately equal attractive forces. For a long, square toothpaste box, the energy density is negative, four sides have attractive (inward) pressures equal to the energy density, and the two ends have repulsive (outward) pressures equal to minus the energy density [25].

Figure 11(a) shows a two-dimensional contour plot of the zero-force surfaces for $a_3 = 1$. The $F_1 = 0$ ($F_2 = 0$) contour is concave toward the $a_2$ ($a_1$) axis. Also shown in this figure is the approximately triangular contour for the zero energy $e = 0$. From this figure one can see, for example, the following. (a) If both $F_1$ and $F_2$ are negative, then $e$ may be positive or negative. (b) If only $F_1$ is negative, $e$ may be positive or negative. (c) If no forces are negative, then $e$ is positive. (d) There are no regions in which all forces are negative. Figure 11(b) shows the corresponding contours in the rotated coordinate system for $a_3' = 3$.
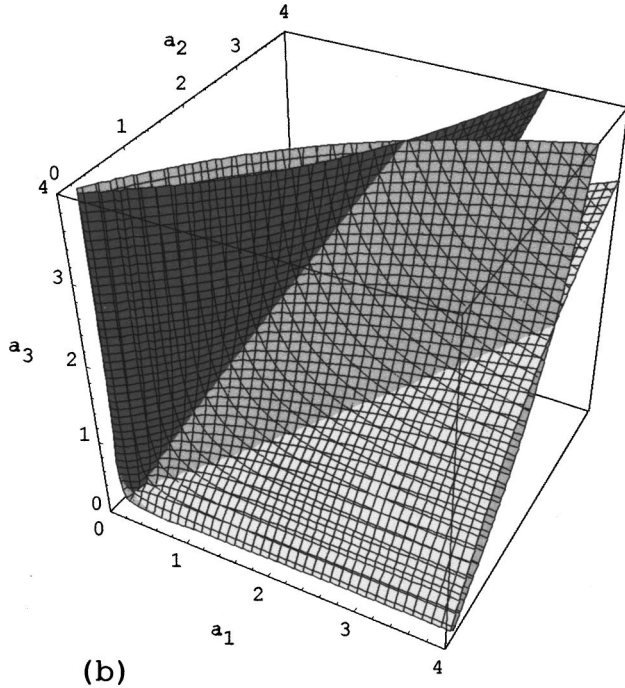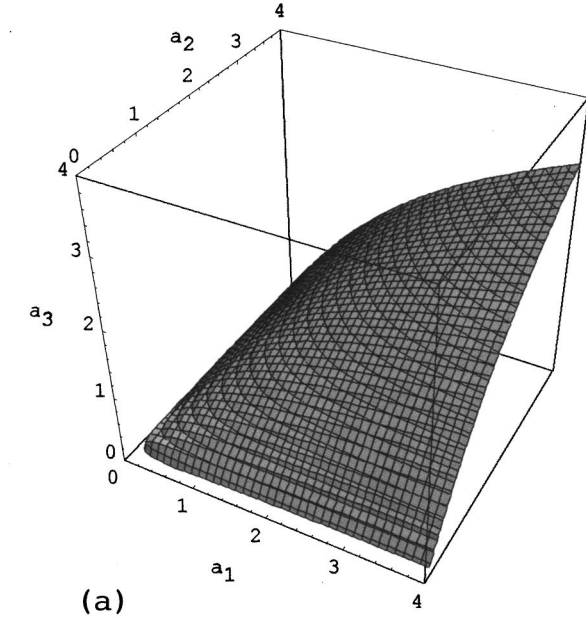


FIG. 9. The energy $e(\boldsymbol{a})$ as a function of $a_1$ and $a_2$ for $a_3 =$ (a) 0.5, (b) 1.0, (c) 3.5, respectively.

The value of $\Phi_3$ can be obtained by noting that $e(a, a, a_3) = e(1, 1, a_3/a) = 0$. For this energy to vanish, we compute $a_3/a = 0.408$ and $3.48$. The smaller value corresponds to the adjacent surface of $S_0$ which is visible in Fig. 1, and the larger value to the portion of the zero-energy surface that is hidden from view. We find $\Phi_3 = 16.1°, 67.9°$.

(a)



(b)

FIG. 10. Contours of zero force. (a) $F_3(\boldsymbol{a})=0$. The force $F_3(a_1,a_2,a_3)$ is negative for points $(a_1,a_2,a_3)$ on the concave side of this surface. (b) Intersecting surfaces for $F_1=0$, $F_2=0$, $F_3=0$. These surfaces define regions in which forces have characteristic signs, for example, in the region that includes the symmetry axis all forces are positive.

There is no geometry for which all forces are zero, and thus there is no local maximum or minimum value of $e(\boldsymbol{a})$, and there are no stable rectangular cavities without introducing some material properties. Casimir attempted to model the electron as a spherical shell of charge held together by



**(a)**



**(b)**
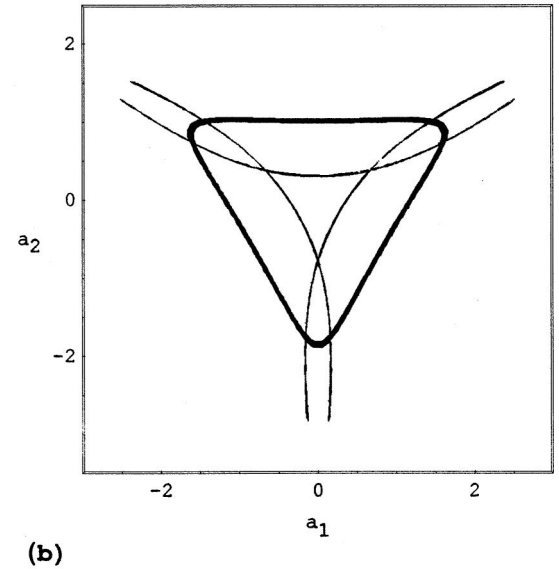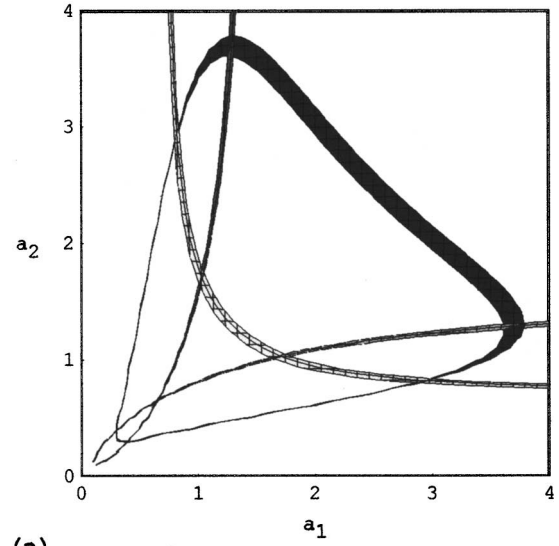
FIG. 11. Contour plots of the zero-force surfaces and the zero-energy surface for (a) $a_3=1.0$; (b) $a_3'=3.0$ (rotated coordinate system). The curve concave toward the $a_2$ axis is $F_1=0$. The bold black lines correspond to the zero-energy surface.

vacuum stresses, but the stress was computed to be outward, resulting in instability. Our results show that a rectangular box also cannot provide a stable structure with attractive forces on all faces, but suggest that perhaps a torus could be stable [39].

We have computed constant-force surfaces for a representative set of forces. Figure 12 shows a set of contours of constant force $F_2$ ranging from $-5$ to $+50$ ($F_1$ and $F_3$ would have the same shape but would be rotated). The four positive forces are on the side of the zero-force contour that includes the line $a_1=a_2=a_3$. Every positive surface has a transition region in which it bends about $90°$ away from the $F=0$ surface. The most negative values of $F_2$ (near $0 \lesssim a_2$) correspond to the attractive force on the large surface in the parallel-plate (pizza box) configuration. The most
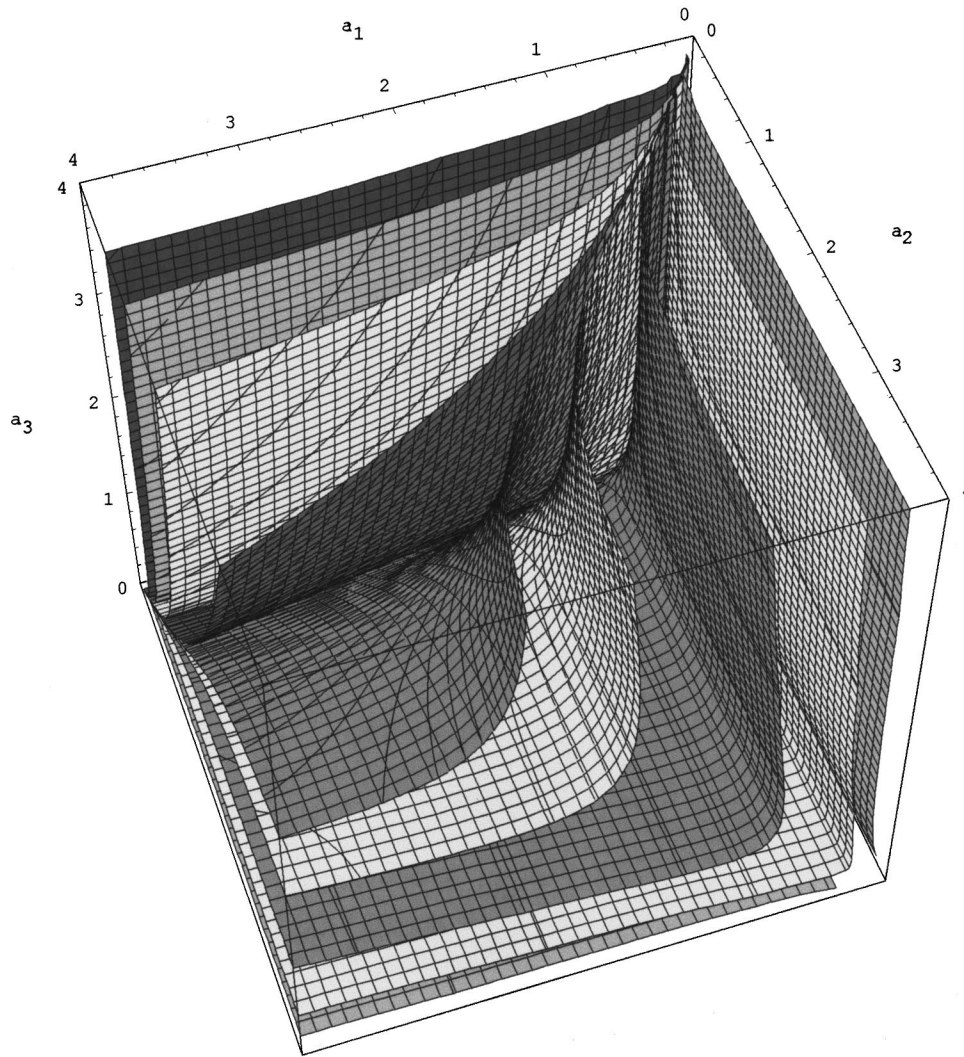
FIG. 12. Contours of constant force $F_2(\boldsymbol{a}) = -5.0, -0.5, -0.05, 0.0, 0.005, 0.05, 0.5, 5.0, 50.0$, where the contours are labeled in order from the top left corner down, from $-5$ to $+50$.

positive values of $F_2$ (near $0 \lesssim a_1$ or $0 \lesssim a_3$) correspond to the four surfaces around the edge of the pizza box.

If we take slices with $a_3$ constant through the set of constant-force contours for $F_2$ in Fig. 12, and similar sets for $F_1$ and $F_3$, we obtain a set of two-dimensional contour surfaces. Figure 13 shows these contours as functions of $a_2$ and $a_3$ for $a_1 = 1$. The thick line represents the contour of zero force. The transition regions for $F_1$ and $F_3$ are clearly visible. Also shown are the contours of constant energy. The thick line with a triangular shape is the zero-energy contour. The dark regions near the axes represent the regions of large positive and negative forces. These two-dimensional contour plots can be obtained from graphs of the forces $F_1, F_2, F_3$ as functions of $a_2$ and $a_3$, for a fixed value of $a_3 = 1$, which are shown in Fig. 14. $F_1$ and $F_2$ are simply rotated versions of each other, and $F_3$ becomes positive whenever $a_3 \gg a_2$ or $a_3 \gg a_1$, which corresponds to one of the long sides in the usual pizza box configuration. A contour plot of the magnitude of the total force is shown in Fig. 15, in which the largest values of $F$ are closest to the axes, and the smallest values of $F$ are in the central region in which shapes are approximately cubical.

In order to understand physically the appearance of positive forces in some of the characteristic rectangular cavities mentioned in the previous paragraph, we consider the mode densities. The mode density near a curved surface has been shown to vary as the radius of curvature [18]. For a right angle of a conductive material, the mode density in the immediate region of the right angle is very high; in fact, it is infinite without a frequency cutoff, leading to a high positive vacuum energy concentrated in the region. The vacuum forces are such that they try to open the right angles to create a flat region. In the cavity geometries in which one or two sides are much smaller than the other sides, several right angles are adjacent and the combined effect of the increased mode density appears to be a local net positive energy density and an outward force on the surface lying between the right angles. This interpretation might provide a rough physical picture for the outward forces predicted for a pizza box geometry and a toothpaste box geometry. However, it may not be applicable since no explicit account was taken of the effects of the intersecting conductive planes in the energy analysis.
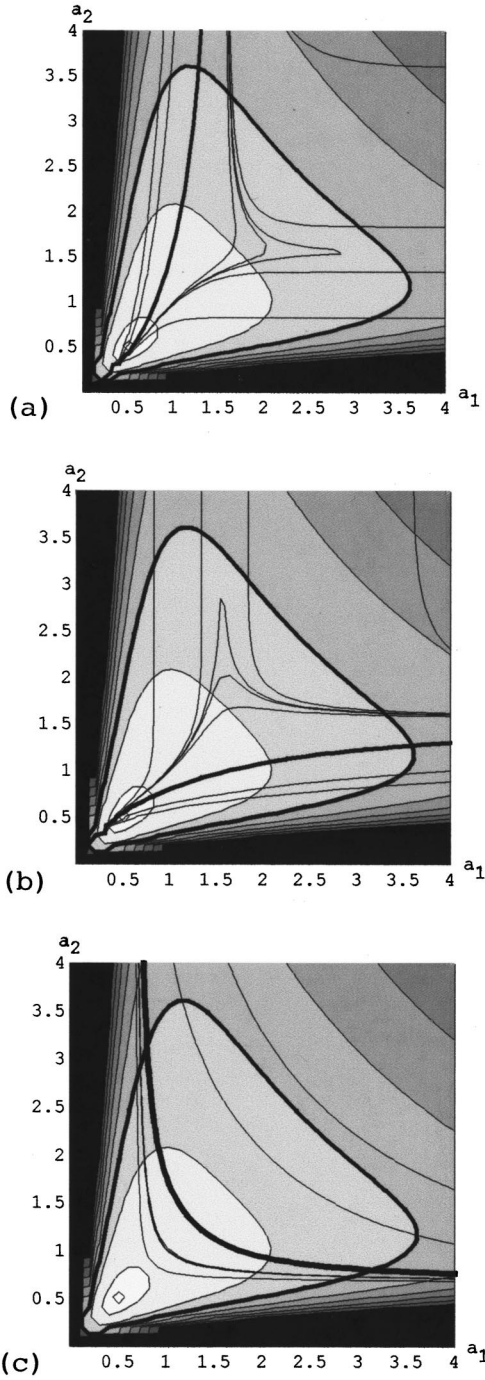
(a)

(b)

(c)

FIG. 13. Constant-energy contours for $a_3=1$ superimposed on the constant-force contour for (a) $F_1=0$; (b) $F_2=0$; (c) $F_3=0$. The triangular-shaped bold line is the zero-energy contour. The other bold line is the zero-force contour. Constant-energy contours correspond to energy values equal to $-0.25, -0.2, -0.15, -0.1, -0.05, 0.0, 0.05, 0.1, 0.111$. Constant-force contours correspond to force values equal to $-0.2, -0.1, 0.0, 0.03, 0.031, 0.0312, 0.032, 0.05$.

It is useful to plot graphs of the forces and energy for several specific, representative geometries. For the geometries $1 \times 0.5 \times a_3$, $1 \times 1 \times a_3$, and $1 \times 3.5 \times a_3$, Fig. 16 shows the variation of the forces and the energy with $a_3$. It is apparent that the energy and the forces vary approximately linearly with $a_3$ for $a_3 > a_2, a_1$. In this linear range, the de-



(a)

(b)

(c)
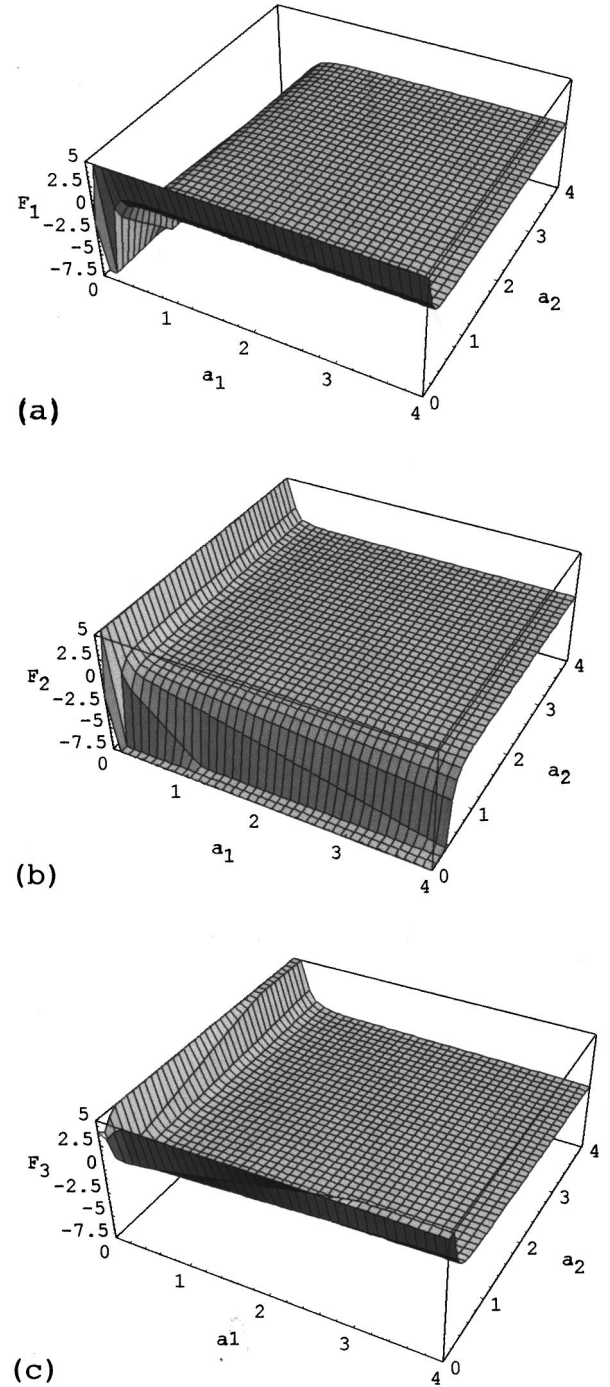
FIG. 14. Forces plotted as function of $a_1, a_2$, for $a_3=1.0$: (a) $F_1$; (b) $F_2$; (c) $F_3$.

rivative of the energy with respect to $a_3$ yields the constant force $F_3$. At the maximum of the energy curve, $F_3$ vanishes. The maximum energy values for the three geometries occur at $a_3=0.5, 0.75, 1.25$, respectively. As the energy peaks shift to larger $a_3$, the peak energy and the slope of the energy curve both decrease. The region in which the energy is positive first increases and then decreases. Indeed, for the $1 \times 3.5 \times a_3$ geometry, the energy peak is almost zero, and for aspect ratios greater than 3.5, the energy is never positive. For most values of $a_3$, two forces are positive or two forces
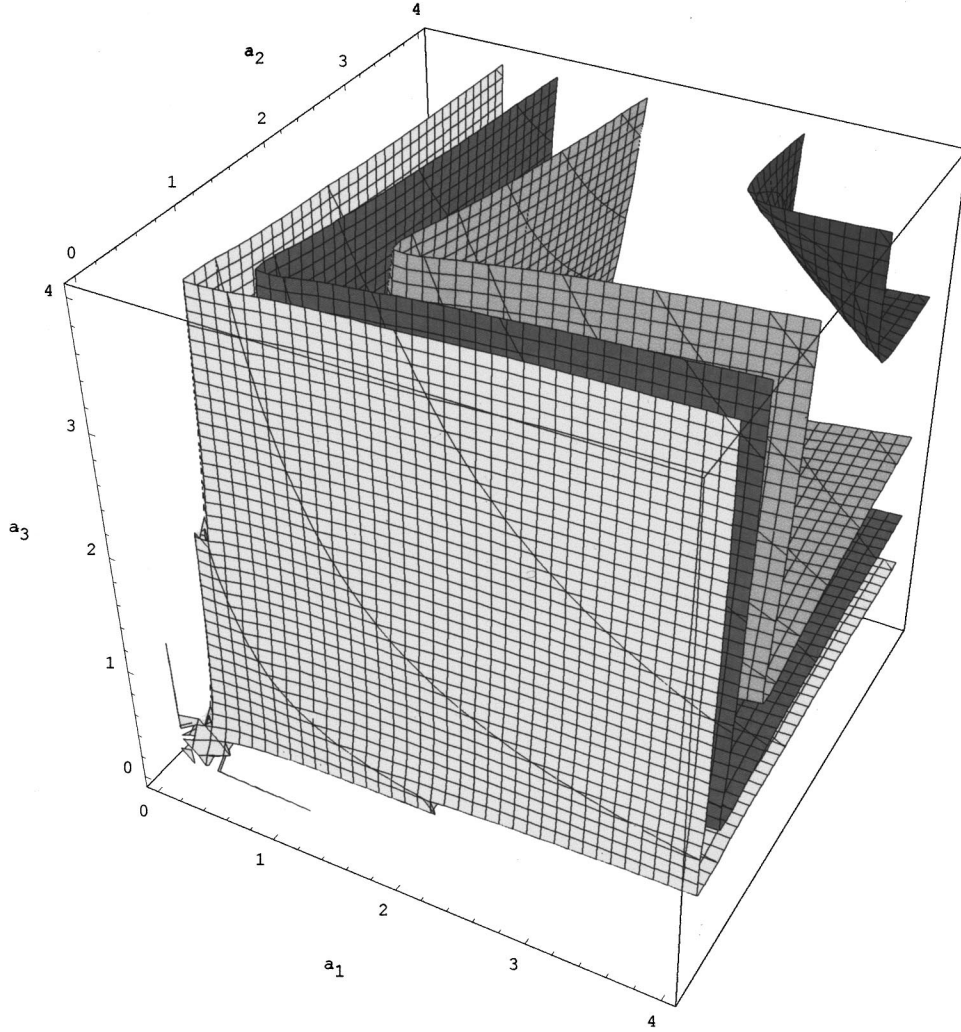
FIG. 15. Contours of constant magnitude of the total force $|F|$. Contours are shown for $|F|$ equal to 5.0,0.5,0.05,0.005.

are negative. Only for the $1\times1\times a_3$ geometry is there a region in which all forces are positive $(0.75<a_3<1.6)$. In Fig. 17, we have plotted the energy density and the pressure for the same geometries as in Fig. 16.

Some general mathematical results may be obtained for constant-force surfaces. If we apply Euler's theorem to the homogeneous functions $F_i$, we obtain

$$\boldsymbol{a}\cdot\boldsymbol{\nabla}_a F_i(\boldsymbol{a})=-2F_i(\boldsymbol{a}). \tag{19}$$

If we multiply by $a_i$ and sum over $i=1,2,3$, and use Eqs. (4) and (10), we obtain a second-order partial differential equation for $e(\boldsymbol{a})$:

$$\sum_{i=1}^{3}\sum_{j=1}^{3}(a_i a_j \partial^2/\partial a_i a_j-2)e(a_1,a_2,a_3)=0. \tag{20}$$

Equation (2) can be expressed as an eigenvalue equation in terms of the scalar operator $f_a$ for the component of the force $\boldsymbol{F}$ along $\boldsymbol{a}$, the principal diagonal of the box. Defining

$$f_a=-\boldsymbol{a}\cdot\boldsymbol{\nabla}_a, \tag{21}$$

we find $f_a e(\boldsymbol{a})=e(\boldsymbol{a})$, and Eq. (20) becomes

$$(f_a^2-1)e(\boldsymbol{a})=0. \tag{22}$$

The operator $i\mu f_a$ is the generator of dilations. The energy $e(\boldsymbol{a})$ is an eigenfunction of this generator, and it transforms under dilations as $e(\boldsymbol{a})\rightarrow e(e^\mu \boldsymbol{a})\rightarrow e^{-\mu}e(\boldsymbol{a})$. In terms of the usual quantum mechanical operators, the force $F_i$ is analogous to the momentum $p_i$ and the torque to the angular momentum.

Equation (2) can be solved to obtain the form of $e(\boldsymbol{a})$ for a cube. For this case, and for the general case, since Eq. (20) is a homogeneous equation that is linear in $e(\boldsymbol{a})$, the boundary conditions must provide the information for the proper numerical factors. One boundary condition that removes any additive constants is that the energy vanishes at infinity. A second condition, such as the value of the energy for a specific cube or for the parallel-plate geometry, appears necessary to secure the proper factors.

## IV. CONCLUSION

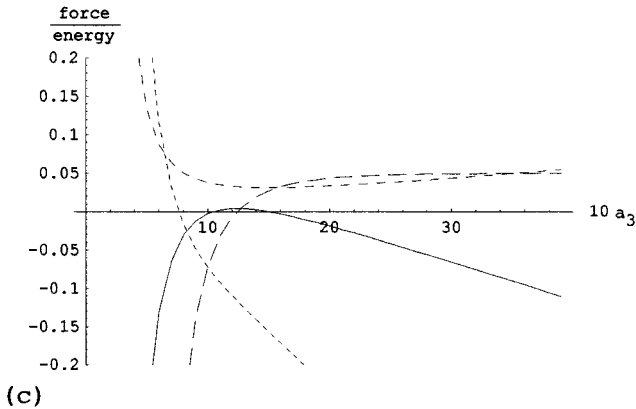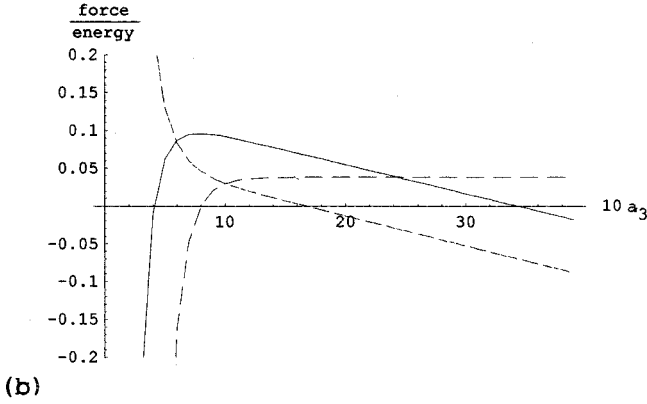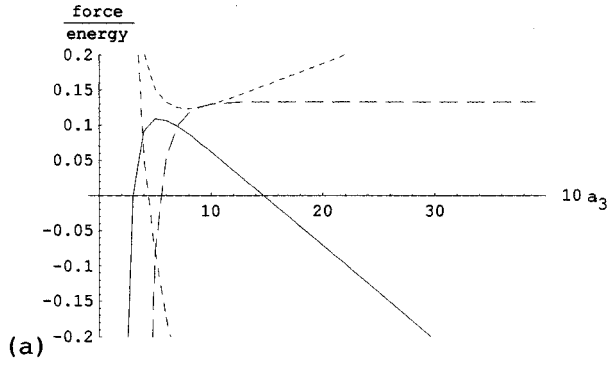By consideration of the symmetry of vacuum energy for a rectangular cavity, we have been able to derive general re-

FIG. 16. Forces ($F_1$, short-dashed line; $F_2$, medium-dashed line; $F_3$, long-dashed line) and energy $e(a)$ (solid line) as a function of $a_3$ for cavities with dimensions (a) $1\times0.5\times a_3$; (b) $1\times1\times a_3$; (c) $1\times3.5\times a_3$.

FIG. 17. Pressures ($P_1$, short-dashed line; $P_2$, medium-dashed line; $P_3$, long-dashed line) and energy density (solid line) for the same cavity dimensions as in Fig. 16: (a) $1\times0.5\times a_3$; (b) $1\times1\times a_3$; (c) $1\times3.5\times a_3$. Note the ordinate scales are different for each graph.

sults that aid in understanding the dependence of the vacuum energy and force on the dimensions of the cavity. The energy is a homogeneous function of the dimensions, which leads to a relationship between the forces and the energy $e(a)=a\cdot F(a)$. This equation provides a direct geometrical link between the energy and the forces, and from it follows the traceless nature of the stress-energy tensor. It may help resolve some of the uncertainties in the definition of a physically meaningful vacuum energy [16]. The forces $F$ are normal to the surfaces of constant energy. Graphing these surfaces in three dimensions displays the $C_{3v}$ symmetry.
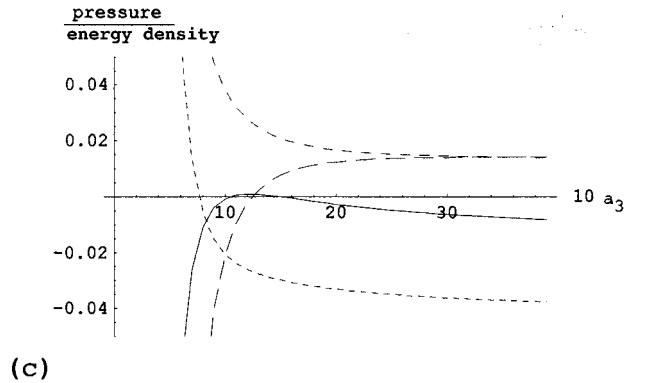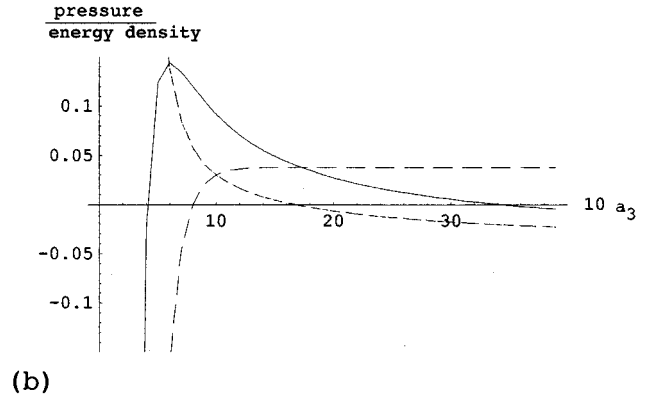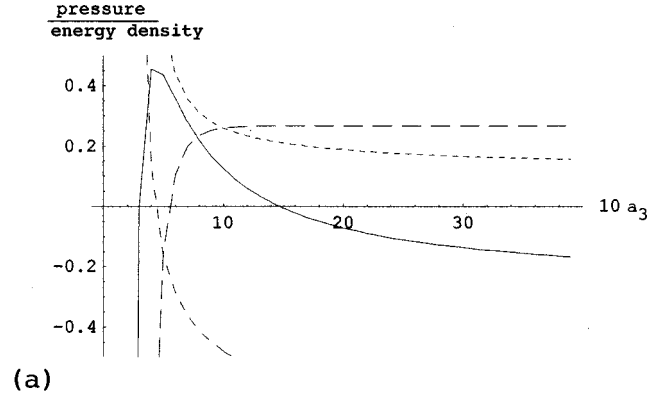
Surfaces of constant positive energy (constant negative energy) are transformed into each other using scale changes. Constant-energy surfaces were also plotted in a rotated coordinate system in which the new $a_3'$ axis is the symmetry axis of the constant-energy surfaces. The contours of constant energy for $a_3'=$const (constant perimeter) show the $C_{3v}$ symmetry about the origin, and show that the maximum energy occurs for a cube at $(0,0,a_3')$. There is no cavity configuration for which all forces vanish (or are negative), so

there is no local maximum or minimum of the energy function. Only for the cube are all forces equal and we may consider the average energy density as being isotropic.

The force on each face of the cavity is also a homogeneous function of the dimensions. Surfaces of zero force and the surface of zero energy, which are all invariant under dilations, divide the space spanned by the vectors *a* into three types of regions with well-defined characteristics. (There are a total of nine different regions, three equivalent regions for each axis.) The three regions are as follows. (1) A region in which the forces and the energy are positive, and the geometry is cubical or nearly cubical. (2) A region in which two forces are positive, one is negative, and the geometry is like a cake box or a pizza box, with the attractive force on the largest side, and the repulsive forces on the smaller sides, and the energy can have either sign depending on the aspect ratio. (3) A region with two negative forces and one positive force, in which the geometry is like a toothpaste tube, the positive force being on the ends, and the energy can have either sign depending on the aspect ratio.

Given the energy for a cube, it appears that it may be possible to obtain other geometries with the same energy by a suitable $C_{3v}$ symmetry coordinate transformation. It might be possible to expand the symmetry group to include transformations to other energy representations of $C_{3v}$. If this were accomplished, one might be able to generate all values of $e(a_1,a_2,a_3)$ from one particular value of $e$ using the operators of this expanded group.

One of the puzzles that remains is the physical explanation of what determines the sign of the vacuum force. For example, why is the vacuum stress positive for the sphere, the cube, and similar configurations? One approach to this conundrum is to consider the number of modes present. For a sphere, using the results of Balian and Duplantier [17], one computes that $\frac{1}{4}$ additional modes are present when the sphere is put in the vacuum field. Hence the vacuum energy is positive. Although mathematically correct, the notion of a fractional mode is perplexing, and Deutsch and Candelas [16] maintain that the cutoff used by Balian and Duplantier [17] to derive their mode function is unphysical. In Ref. [40] Hushwater explained the repulsive Casimir forces in parallel plate geometries as due to the redistribution of the free field vacuum modes that occurs with the boundary conditions for the geometry. For the case of a perfectly conducting and an infinitely permeable plate he showed the repulsive force arises from the curvature of the mode function. One issue in his explanation is that the curvature leading to the repulsive force is due entirely to the frequency cutoff function used.

Negative energy densities tend to appear in ''asymptotic'' cases, that is, when at least one dimension is a factor of 2 or more smaller than the other dimensions. This suggests that the most important factor leading to negative energy densities may be mode exclusion. On the other hand, positive energy densities tend to occur when all dimensions are of similar magnitude, suggesting that the most important factor may be the constructive relationship between the electric and magnetic fields in the three orthogonal directions.

It may be of some value to understand what causes a positive energy density and positive forces and negative forces in order to optimize geometries. Many other puzzles with vacuum fluctuations remain. With an increased understanding of vacuum forces and energy in rectangular cavities, including the effects of temperature, it may be possible to engineer micromachined devices to measure the repulsive forces and to make useful structures that utilize vacuum energy and Casimir forces. Biological structures, for example, microtubules in cell cytoskeletons, the endoplasmic reticulum, or diatoms, may have functions that involve interaction with the vacuum field.

[1] H. B. G. Casimir, K. Ned. Akad. Wet. Proc. **51**, 793 (1948).

[2] P. Plunien, B. Muller, and W. Greiner, Phys. Rep. **134**, 87 (1986).

[3] H. Bethe, Phys. Rev. **72**, 339 (1948).

[4] T. Welton, Phys. Rev. **74**, 1157 (1948).

[5] J. Schwinger, L. DeRaad, Jr., and K. Milton, Ann. Phys. (N.Y.) **115**, 1 (1978).

[6] P. Milonni, *The Quantum Vacuum* (Academic, San Diego, 1994), p. 239.

[7] M. Sparnaay, in *Physics in the Making*, edited by A. Sarlemijn and M. Sparnaay (Elsevier, Amsterdam, 1989). See also D. Tabor and R. H. S. Winterton, Proc. R. Soc. London, Ser. A **312**, 435 (1969). References [2] and [27] provide additional experimental references.

[8] E. M. Lifshitz, Zh. Éksp. Teor. Fiz. **29**, 94 (1956) [Sov. Phys. JETP **2**, 73 (1956)]. See also Ref. [26] for correction of some errors by Lifshitz.

[9] S. Lamoroux, Phys. Rev. Lett. **78**, 5 (1997).

[10] U. Mohideen and Roy Anushree, Phys. Rev. Lett. **81**, 4549 (1998).

[11] M. Serry, D. Walliser, and J. Maclay, J. Appl. Phys. **84**, 2501 (1998).

[12] M. Serry, D. Walliser, and J. Maclay, J. Microelectromech. Syst. **4**, 193 (1995).

[13] J. Maclay, M. Serry, R. Iliac, P. Neural, and D. Czaplewski, NASA Report No. NASA/CP-1999-208694.

[14] B. DeWitt, in *Physics in the Making* (Ref. [7]).

[15] L. Brown and J. Maclay, Phys. Rev. **184**, 1272 (1969).

[16] D. Deutsch and P. Candelas, Phys. Rev. D **20**, 3063 (1979).

[17] R. Balian and B. Duplantier, Ann. Phys. (N.Y.) **112**, 165 (1978).

[18] J. Dowker and G. Kennedy, J. Phys. A **11**, 895 (1978).

[19] W. Lukosz, Z. Phys. **262**, 327 (1973).

[20] P. Candelas, Ann. Phys. (N.Y.) **143**, 241 (1982). This paper also discusses the infinite energy that arises at the interface between different dielectrics.

[21] S. Lamoreaux, Phys. Rev. A **59**, R3149 (1999).

[22] See P. Milonni and M. Shih, Contemp. Phys. **33**, 313 (1992) for an approximate computation using a pairwise integration of van der Waals forces for parallel plates yielding 80% of the correct value. P. Milonni and H. Fearn have used this method to get approximate forces for other geometries as well (private communication).

[23] K. Milton, L. DeRaad, and J. Schwinger, Ann. Phys. (N.Y.) **115**, 388 (1978).

[24] T. Boyer, Phys. Rev. **174**, 1764 (1968).

[25] W. Lukosz, Physica (Amsterdam) **56**, 109 (1971).

[26] J. Ambjorn and S. Wolfram, Ann. Phys. (N.Y.) **147**, 1 (1983).

[27] S. Hacyan, R. Jauregui, and C. Villarreal, Phys. Rev. A **47**, 4204 (1993).

[28] V. Mostepananko and N. Trunov, *The Casimir Effect and Its Applications* (Clarendon Press, Oxford, 1997), p. 40.

[29] J. Schwinger, L. DeRaad, Jr., and M. Kimball, Ann. Phys. (N.Y.) **115**, 1 (1978).

[30] E. Elizalde and A. Romero, Am. J. Phys. **59**, 711 (1991).

[31] H. Bateman, *Higher Transcendental Functions* (McGraw-Hill, New York, 1955), Vol. III, p. 195.

[32] E. Whittaker and G. Watson, *A Course in Modern Analysis* (Cambridge University Press, London, 1963), p. 52.

[33] M. Schaden and L. Spruch, Phys. Rev. A **58**, 935 (1998).

[34] R. Crandall and J. Buhler, J. Phys. A **20**, 5497 (1987); R. Crandall (unpublished). Wolfram Research very kindly provided a MATHEMATICA version of the algorithm.

[35] We could also use the symmetric group of permutations of three objects $S_3$.

[36] P. Morse and H. Feshbach, *Methods of Theoretical Physics* (McGraw-Hill, New York, 1953), Vol. 1, pp. 6 and 14.

[37] We use the metric signature $(-1,1,1,1)$.

[38] T. Apostol, *Mathematical Analysis* (Addison-Wesley, Reading, MA, 1957), p. 134.

[39] There is some confusion in the literature regarding the stability of rectangular cavities. X. Li, H. Cheng, J. Li, and X. Zhai, Phys. Rev. D **55**, 4940 (1997) concluded incorrectly that a rectangular cavity would be stable if had a negative energy density. This error arises from the assumption of an isotropic energy density. R. Weigand and J. Guerra also made this error in their analysis, Eur. J. Phys. **18**, 40 (1997).

[40] V. Hushwater, Am. J. Phys. **65**, 381 (1997).